

ChemComm

Accepted Manuscript



This is an *Accepted Manuscript*, which has been through the Royal Society of Chemistry peer review process and has been accepted for publication.

Accepted Manuscripts are published online shortly after acceptance, before technical editing, formatting and proof reading. Using this free service, authors can make their results available to the community, in citable form, before we publish the edited article. We will replace this *Accepted Manuscript* with the edited and formatted *Advance Article* as soon as it is available.

You can find more information about *Accepted Manuscripts* in the [Information for Authors](#).

Please note that technical editing may introduce minor changes to the text and/or graphics, which may alter content. The journal's standard [Terms & Conditions](#) and the [Ethical guidelines](#) still apply. In no event shall the Royal Society of Chemistry be held responsible for any errors or omissions in this *Accepted Manuscript* or any consequences arising from the use of any information it contains.

COMMUNICATION

Mössbauer and computational investigation of a functional [NiFe] hydrogenase model complex

Cite this: DOI: 10.1039/x0xx00000x

A. Kochem,^a E. Bill,^a F. Neese^a and M. van Gastel^{a,*}

Received 00th January 2012,

Accepted 00th January 2012

DOI: 10.1039/x0xx00000x

www.rsc.org/

Developing biomimetic complexes that model the active site of [NiFe] hydrogenase enzymes in order to catalyze the activation of H₂ is a topic of major interest. A functional [NiFe] Hydrogenase model complex has recently been described by Ogo et al (*Science*, 2013, 339, 682-683). Here, we report a Mössbauer and computational investigation of this model complex. This study affords deeper understanding of the electronic structure, the reactivity and the mechanism of H₂ activation by this complex.

The search for cheap and durable catalysts for energy storage is of vital importance. For this reason, many inorganic chemistry groups focus their research efforts on the synthesis and investigation of bio-inspired catalyst molecules¹ in the hope that these molecules can catalyze the production of H₂ with a turnover frequency and overpotential approaching that of native biological systems like hydrogenases,² or that of platinum metal.^{3,4} Recently, a functional [NiFe] mimic that catalyzes hydride transfer from H₂ has been reported in the group of Ogo et al.⁵ The crystal structure of this diamagnetic complex **1** with formal valences Ni(II) and Fe(II) shows a relatively long Ni-Fe distance of 3.319 Å. The Ogo complex **1** is able to bind and heterolytically split H₂ in the presence of a base, yielding a ferrous hydride complex **2** with a shorter Ni(II)-Fe(II) distance of 2.793 Å. The Ni-H-Fe linkage is additionally very asymmetric with Fe-H and Ni-H distances of 1.57(5) Å and 2.16(4) Å, respectively.⁵ In comparison, recent hydrido complexes from the Rauchfuss group either feature a shorter Ni(II)-Fe(II) distance that affords the presence of a direct metal-metal bond at about 2.6 Å,⁶ and mimics that observed in the Ni-R state (Ni(II)-Fe(II) with a bridging hydride) of [NiFe] hydrogenases,⁷ or feature a long Ni(II)-Fe(II) distance of 3.218 Å.⁸ The Ni-H-Fe linkages in these models were also asymmetric with the Fe-H distance being shorter than the Ni-H distance by up to 0.37 Å depending on the surrounding ligands.^{6,8} Still, with these large variations in Ni-Fe distances, it remains unclear in **2**, how H₂ is split by this complex, whether the hydride is better described as a bridging or a terminal hydride,

whether or not both metals can bind a hydride, and how the electronic structure of the complex is best understood. So far, calculations on an analogous complex featuring nickel and ruthenium have shown that a hydrogen bonded network of polar solvent molecules (water in the latter case, which also functioned as a base) may greatly assist in the reaction.⁹ In this communication, we address these topics by a combination of Mössbauer spectroscopy, which is ideally suited to probe the electronic structure near Fe, and quantum chemistry.

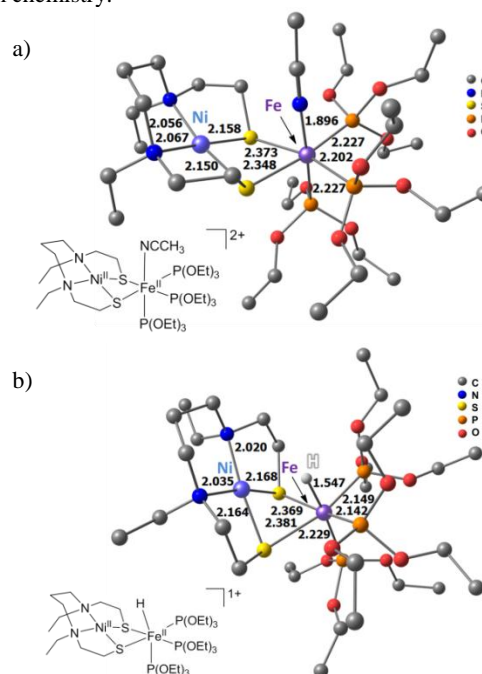


CHART. 1 Geometry optimized structure of a) **1** and b) **2** and selected bond distances. H atoms are omitted except those of the hydride for clarity.

Both compounds, **1** and **2**, were studied by Mössbauer spectroscopy which is sensitive to oxidation state and to local spin state and to the electron density and changes thereof at the iron. At 80 K and zero magnetic field, **1** exhibits a quadrupole doublet with relatively low isomer shift and small quadrupole splitting ($\delta = 0.25$ mm/s, $\Delta E_Q = 0.24$ mm/s, Fig. 1). Under the same conditions, **2** exhibits a significantly lower isomer shift and a much larger quadrupole splitting ($\delta = 0.18$ mm/s, $\Delta E_Q = 1.52$ mm/s, Fig. 1). Both isomer shift values are typical of low-spin iron sites. Calculated isomer shifts and quadrupole splittings which were derived from DFT calculations¹⁰ are shown in Table 1 and are in excellent agreement with experimental data.

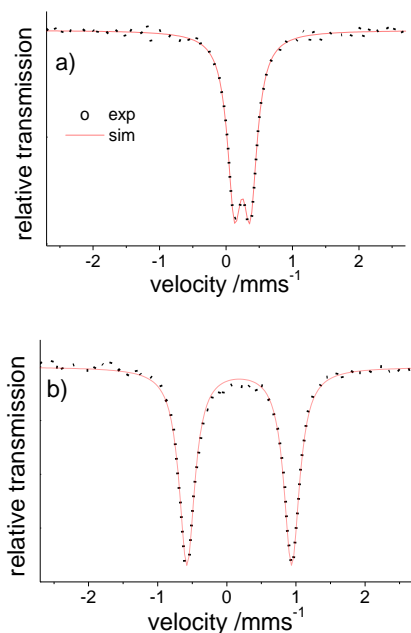


Fig. 1 Mössbauer spectrum of a) **1** and b) **2** recorded at 80 K without an applied field. The given shift is relative to α -Fe. Fitted parameters for **1**: $\delta = 0.25$ mm/s, $\Delta E_Q = 0.24$ mm/s, and for **2**: $\delta = 0.18$ mm/s, $\Delta E_Q = 1.52$ mm/s.

Early Mössbauer investigations of [NiFe]-hydrogenases have revealed a spectral component with a low isomer shift, $\delta = 0.005$ - 0.15 mm/s¹¹ which has later been assigned to the low-spin iron(II) center of the active site.¹² The isomer shifts of low-spin iron complexes are generally less sensitive to the coordination environment than those of high-spin complexes.¹³ The differences of the isomer shifts of **1** and **2** mainly arise from σ -donation, π -backdonation or π -accepting properties of the surrounding ligands. Both σ -donation and π -backdonation lead to an increase in s -electron density at the nucleus and give rise to more negative isomer shifts.¹⁴ It is thus interesting to compare the difference of the isomer shifts of **1** and **2**, since it provides information about the covalency of the iron-hydride bond and thereby about the terminal *versus* bridging hydride mode as well as on the hydricity which in turn is directly correlated to the reactivity of the catalyst. The smaller isomer shift of **2** is consistent with the better σ -donating ability of the hydride as compared to acetonitrile. Thus, the significantly smaller isomer shift

of **2** as compared to **1** reflects that the hydride is terminal rather than bridging and therefore covalently bound. This is supported by calculations described below.

The quadrupole splitting provides information about the local charge asymmetry at the iron site. For **2** its absolute value is much larger than for **1**. This is not surprising, since the replacement of a neutral acetonitrile molecule by a mono-anionic and in particular covalently bound hydride drastically changes the electric field gradient (EFG) at the iron. Since the $3d^6$ low-spin configuration of Fe(II) formally does not provide a valence contribution to the EFG, the ligand effect on the quadrupole splitting arises exclusively from anisotropy of the covalent bonds. The calculated orientation of the principal axis system of the EFG tensor of **1** and **2** are given in Fig. S2 and Fig. S3 respectively.

Table 1 Experimental and Calculated Mössbauer Parameters for **1** and **2**.^a

Parameter	1 , exp.	1 , calc.	2 , exp.	2 , calc.
δ , [mm/s]	0.25	0.23	0.18	0.18
ΔE_Q , [mm/s]	0.24	0.29	-1.52	-1.75
η	0.3	0.2	0.4	0.4

^a Experimental details are given in the ESI

In order to provide a clear picture of the electronic structure of **1** and **2**, a computational investigation was carried out using density functional theory (DFT). Scalar relativistic effects were taken into account with the zero order regular approximation (ZORA). Geometry optimizations were performed with the BP86 functional for **1**, **2** (Chart1) and the adducts (**1** without CH_3CN , **1** with coordinated H_2 instead of CH_3CN (**1-H₂**), Fig. S1). The coordination bond distances calculated by geometry optimization match those of the X-ray structures to within 0.05 and 0.03 Å for **1** and **2**, respectively.⁶ The slight over-estimation of the coordinated bond distances is typical for current DFT functionals.¹⁵ In order to validate our models, frequency calculations of the optimized structures have been performed. The Fe-hydride stretching frequency observed experimentally for **2** is well reproduced by calculation (exp: 1687 cm^{-1} , calc: 1743 cm^{-1}) as well as the shift observed when using **2-D** (exp: 1218 cm^{-1} , calc: 1240 cm^{-1}).⁶ No Ni-H stretch vibrations were observed in the calculations. Furthermore, the decrease in the isomer shift and increase in quadrupole splitting from **1** to **2** is well reproduced by the calculations. Of particular interest is the binding mode of the hydride (bridging *versus* terminal). Detailed analysis of the localized orbitals reveals a strongly covalent $1s$ - $3d_z^2$ mixing between the orbitals of the hydride and the iron in **2** (Fig. 2-a). A σ -bond between the nitrogen of the acetonitrile and the iron ($2s$ - $3d_z^2$ mixing) in **1** is also observed but much weaker and in agreement with the lower degree of covalency and larger isomer shift (Fig. 2-b). The Mayer bond orders amount to 0.65 for Fe-H in **2** and to 0.71 for Fe-N in **1**.

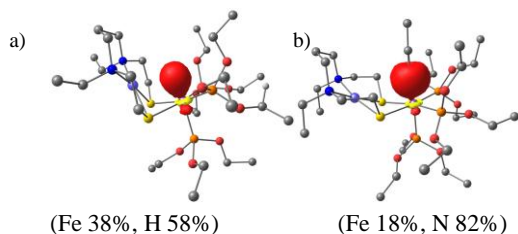


Fig. 2 Localized orbitals between iron and the axial ligand (BP86/def2-TZVP) for complex a) **2** and b) **1**.

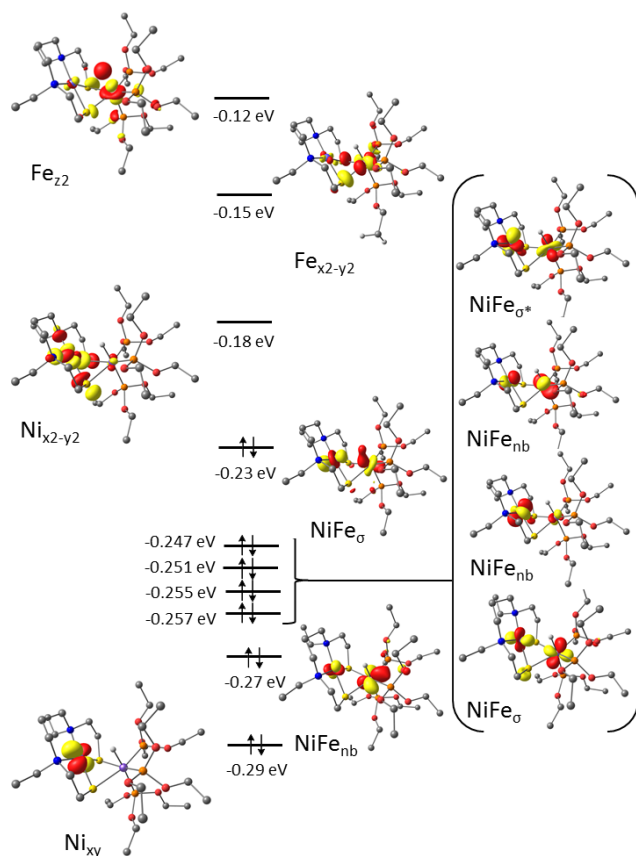


Fig. 3 Calculated frontier orbital diagram for **2** with pictorial representations included (BP86/def2-TZVP/def2-TZVP/ZORA).

Most importantly, the Ni and the hydride don't form a σ -bond and are not in covalent interaction, showing that the hydride is clearly terminal in **2** rather than bridging. The shorter Ni-Fe bond length in **2** (2.7930(6) Å) as compared to **1** (3.3189(6) Å) might result from electrostatic interaction between the hydride and the nickel, bringing the two parts of the complex and the two metal ions closer. Representative molecular orbital diagrams of complexes **2** and **1** with pictorial representations of the frontier molecular orbitals are shown in Fig. 3 and Fig. S4, respectively. The complex **2** adopts a $(\text{Ni}_{xy})^2(\text{NiFe}_{nb})^6(\sigma)^2(\sigma^*)^4$ configuration. From this configuration, the formal bond order between nickel and iron is 0, in agreement with the calculated Mayer bond (MBO) order of 0.124.

Experimentally, **1** was shown to bind and heterolytically split H_2 in the presence of a strong base (MeONa) to provide the hydrido complex **2** which is then able to react with a strong acid

(HBF_4) to produce H_2 and give back the complex **1**.² In order to provide more understanding of the reactivity of this complex we computationally investigated the mechanism of H_2 activation. The calculated reaction pathway for heterolytic splitting of H_2 is shown in Fig. 4 and begins with the binding of the H_2 molecule to the iron center. The transformation of **1** to **1-H₂** where H_2 is bound side-on to Fe(II), is only about 4 kcal/mol uphill. Then a MeO^- base attacks the dihydrogen in **1-H₂** and immediately forms a methanol molecule (i.e., activationless, without transition state) and the corresponding hydrido complex **2** by taking a proton from H_2 . This strongly exothermic step was found to be barrierless. We calculated the reaction enthalpy formation of the hydrido species **2** from **1** to be exothermic by 35 kcal/mol in the presence of H_2 and a strong base.

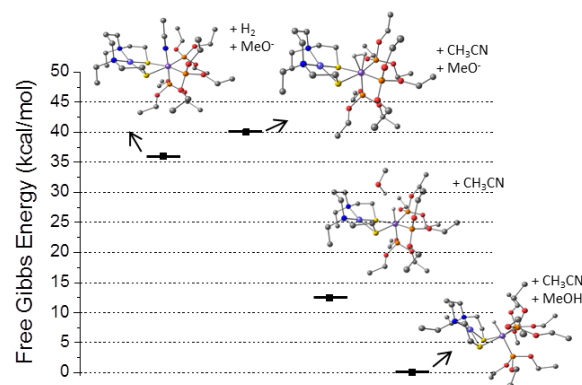


Fig. 4 Gibbs free energy H_2 splitting pathway calculated for **1** with CH_3O^- .

The calculated reaction pathway for H_2 production is shown Fig S5. The reaction proceeds such that the hydride bound in **2** is protonated by the acid and forms the corresponding complex **1-H₂**. The reaction enthalpy formation of the species **1-H₂** was also found to be exothermic by 30 kcal/mol in the presence of HBF_4 . The reaction then proceeds by elimination of H_2 to form **1** and H_2 (-5 kcal/mol, again activationless). In order to gain more information about the reactivity of this complex with respect to the pKa of the acid and whether transition states may occur, we additionally investigated the reaction pathway for H_2 activation with $\text{CH}_3\text{COOH}/\text{CH}_3\text{COO}^-$ (Fig. 5). The energy profile indicates that the reaction is in favor of H_2 splitting rather than the H_2 production. The deprotonation of the species **1-H₂** by CH_3COO^- to give **2** and CH_3COOH is indeed exothermic by 7.5 kcal/mol and the reaction has a barrier of 2.7 kcal/mol. The geometry optimized structure of the transition state is provided in the supporting information. In this regards, we point out that the hydricity of **2** is not large enough to react with such a weak acid and that the reactivity of the complex for the H_2 activation is in favor of the H_2 splitting.

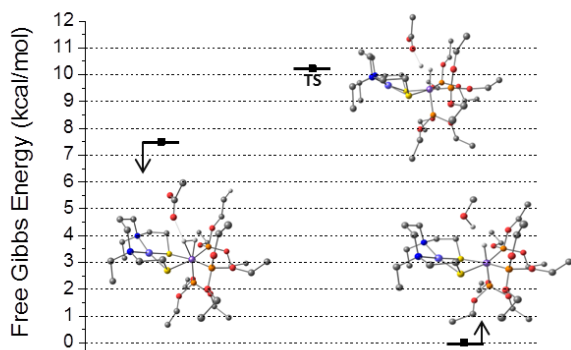


Fig. 5 Gibbs free energy H_2 splitting pathway calculated for **1** with CH_3COO^- .

In summary, both the Mössbauer data and the quantum chemical calculations indicate that the hydride in **2** is terminal rather than bridging. As such, the complex **1** is able to function as a hydride acceptor, and it also able to bind H_2 , two important properties for a putative molecular hydrogen evolving catalyst. The actual role of the complex as a catalyst for hydrogen activation is doubtful in its present form: for hydrogen splitting, **1**- H_2 transforms into **2** in an activationless process after addition of even a weak base (cf. Fig. 5). Presently, hydrogen production from **2** can only be driven if a strong acid like HBF_4 is present. The activity of the complex would improve by changing the system such that **2** would be destabilized, thus raising the energy of the right-most level in Fig. 5. It is presently not clear what the role of the nickel atom is, since it apparently neither plays a role in the binding of H_2 or H^- . One suggestion is that the square planar nickel has a shielding function and provides a hydrophobic environment for the hydride.⁵ Electronically, manipulation of the ligand periphery at the nickel site by introduction of a soft, electron-delocalizing ligand may additionally stabilize the Ni $d_{x^2-y^2}$ based electron acceptor orbital (Fig. 3). It thus increases the electronegativity of nickel, thereby weakening the Fe-H bond, since the metals are more in competition over for the hydride. Additionally, the complex presently lacks a proton shuttle, the introduction of which has proven its merit in a series of highly active nickel-phosphine catalysts from DuBois et al.¹ In its present conformation, H_2 splitting is favored.

Notes and references

^a Max Planck Institute for Chemical Energy Conversion, Stiftstrasse 34-36, D-45470 Mülheim an der Ruhr, Germany

Electronic Supplementary Information (ESI) available: [Details of the spectroscopic and computational investigation]. See DOI: 10.1039/c000000x/

- 1 D. L. DuBois, *Inorg. Chem.*, 2014, **53**, 3935-3960.
- 2 (a) A. J. Esswein and D. G. Nocera, *Chem. Rev.*, 2007, **107**, 4022-4047. (b) G. J. Kubas, *Chem. Rev.*, 2007,

107, 4152-4205. (c) P. M. Vignais and B. Billoud, *Chem. Rev.*, 2007, **107**, 4206-4272. (d) J. C. Fontecilla-Camps, A. Volbeda, C. Cavazza and Y. Nicolet, *Chem. Rev.*, 2007, **107**, 4273-4303. (e) A. L. De Lacey, V. M. Fernández, M. Rousset and R. Cammack, *Chem. Rev.*, 2007, **107**, 4304-4330. (f) W. Lubitz, E. Reijerse and M. van Gastel, *Chem. Rev.*, 2007, **107**, 4331-4365. (g) K. Vincent, A. Parkin and F. A. Armstrong, *Chem. Rev.*, 2007, **107**, 4366-4413. (h) P. E. M. Siegbahn, J. W. Tye and M. B. Hall, *Chem. Rev.*, 2007, **107**, 4414-4435.

- 3 J. K. Nørskov and C. H. Christensen, *Science*, 2006, **312**, 1322-1323.
- 4 *Chemical Energy Storage*, ed. R. Schlögl, De Gruyter, Berlin, 2013.
- 5 S. Ogo, K. Ichikawa, T. Kishima, T. Matsumoto, H. Nakai, K. Kusaka and T. Ohhara, *Science*, 2013, **339**, 682-683.
- 6 M. E. Carroll, B. E. Barton, D. L. Gray, A. E. Mack and T. B. Rauchfuss, *Inorg. Chem.*, 2011, **50**, 9554-9563.
- 7 M. Kampa, M.-E. Pandelia, W. Lubitz, M. van Gastel and F. Neese, *J. Am. Chem. Soc.*, 2013, **135**, 3915-3925.
- 8 B. C. Manor, T. B. Rauchfuss, *J. Am. Chem. Soc.*, 2013, **135**, 11895-11900.
- 9 S. Furlan, G. L. Penna, *J. Biol. Inorg. Chem.*, 2012, **17**, 149-164.
- 10 M. Römelt, S. Ye and F. Neese, *Inorg. Chem.*, 2009, **48**, 784-789.
- 11 K. K. Surerus, M. Chen, J. W. van der Zwaan, F. M. Rusnak, M. Kolk, E. C. Duin, S. P. J. Albracht and R. Münck, *Biochemistry*, 1994, **33**, 4980-4993.
- 12 H. F. Hsu, S. A. Koch, C. V. Popescu and E. Münck, *J. Am. Chem. Soc.*, 1997, **119**, 8371-8372.
- 13 P. Gütllich, E. Bill, and A. X. Trautwein, *Mössbauer Spectroscopy and Transition Metal Chemistry*; Springer: Heidelberg, 2011.
- 14 F. Neese, *Inorg. Chim. Acta*, 2002, **337**, 181-192.
- 15 F. Neese, *J. Biol. Inorg. Chem.*, 2006, **11**, 702-711.